applied sciences

MDPI

Article

Biosynthesized Zinc Oxide Nanoparticles Disrupt Established Biofilms of Pathogenic Bacteria

Fohad Mabood Husain [1,*], Faizan Abul Qais [2], Iqbal Ahmad [2], Mohammed Jamal Hakeem [1], Mohammad Hassan Baig [3], Javed Masood Khan [1] and Nasser A. Al-Shabib [1]

[1] Department of Food Science and Nutrition, College of Food and Agriculture Sciences, King Saud University, Riyadh 11451, Saudi Arabia; mhakeem@ksu.edu.sa (M.J.H.); jmkhan@ksu.edu.sa (J.M.K.); nalshabib@ksu.edu.sa (N.A.A.-S.)

[2] Department of Agricultural Microbiology, Faculty of Agricultural Sciences, Aligarh Muslim University, Aligarh 202002, UP, India; faizanabulqais@gmail.com (F.A.Q.); ahmadiqbal8@yahoo.co.in (I.A.)

[3] Department of Family Medicine, Yonsei University College of Medicine, Gangnam Severance Hospital, 211 Eonju-Ro, Gangnam-Gu, Seoul 06273, Korea; baig@yuhs.ac

* Correspondence: fhusain@ksu.edu.sa

Abstract: Global emergence and persistence of the multidrug-resistant microbes have created a new problem for management of diseases associated with infections. The development of antimicrobial resistance is mainly due to the sub-judicious and unprescribed used of antimicrobials both in healthcare and the environment. Biofilms are important due to their role in microbial infections and hence are considered a novel target in discovery of new antibacterial or antibiofilm agents. In this article, zinc oxide nanoparticles (ZnO-NPs) were prepared using extract of *Plumbago zeylanica*. ZnO-NPs were characterized and then their antibiofilm activity was tested against Gram-positive and Gram-negative bacteria. The ZnO-NPs were polydispersed, and the average size was obtained as 24.62 nm. The presence of many functional groups indicated that phytocompounds of *P. zeylanica* were responsible for the synthesis, capping, and stabilization of ZnO-NPs. Synthesized NPs inhibited the biofilm formation of *E. coli*, *S. aureus*, and *P. aeruginosa* by 62.80%, 71.57%, and 77.69%, respectively. Likewise, concentration-dependent inhibition of the EPS production was recorded in all test bacteria. Microscopic examination of the biofilms revealed that ZnO-NPs reduced the bacterial colonization on solid support and altered the architecture of the biofilms. ZnO-NPs also remarkably eradicated the preformed biofilms of the test bacteria up to 52.69%, 59.79%, and 67.22% recorded for *E. coli*, *S. aureus*, *P. aeruginosa*, respectively. The findings reveal the ability of green synthesized zinc oxide nanoparticles to inhibit, as well as eradicate, the biofilms of Gram-positive and Gram-negative bacteria.

Keywords: zinc oxide nanoparticles; *Plumbago zeylanica*; biofilm; EPS; biofilm eradication

Citation: Husain, F.M.; Qais, F.A.; Ahmad, I.; Hakeem, M.J.; Baig, M.H.; Masood Khan, J.; Al-Shabib, N.A. Biosynthesized Zinc Oxide Nanoparticles Disrupt Established Biofilms of Pathogenic Bacteria. *Appl. Sci.* **2022**, *12*, 710. https://doi.org/10.3390/app12020710

Academic Editor: Chih-Ching Huang

Received: 28 November 2021
Accepted: 7 January 2022
Published: 12 January 2022

1. Introduction

Nanotechnology is an emerging field of science that deals with the application of nanomaterial in numerous fields [1]. In nanobiotechnology, the use of nanomaterials is mainly focused in medical diagnostics, drug delivery, agriculture, etc. [2]. The major interest in application of such nanomaterials is due to the fact that at nano scale, these materials exhibit a completely different set of properties encompassing physicochemical, optoelectronic, magnetic, etc. [3]. The very small size of nanoparticles makes their surface area to the volume ratio very large, making them drastically change their catalytic activity, mechanical properties, biological properties, electrical conductivity, etc. [4]. Hence, the researchers are focused on the development of nanomaterials capable of exhibiting novel properties that could be employed in various disciplines of medicine and biology.

There are many commonly used methods of nanoparticles synthesis. Among them, chemical, physical, and biological methods are the most commonly used procedures [5]. In green synthesis, there is the use of natural products, such as plant extracts or microbes,

to produce nanoparticles. The green route of nanoparticle synthesis is advantageous over chemical procedure due to the fact that chemical synthesis uses certain harmful materials and many times produces toxic byproducts [6,7]. This makes the green route an eco-friendly procedure. Moreover, the green synthesis is usually a one-step process, produces relatively stable nanoparticles, and is also more economic than the chemical synthesis [8]. On the contrary, there are also certain drawbacks with the green route of nanoparticles synthesis. The major one is one is that nanoparticles produced in green synthesis are not of precise size and shape and are usually polydispersed in nature. Such variation is because the compounds of plants or microbes act as both reducing and stabilizing agent. There is simultaneous reduction, capping, and stabilization of nanoparticles that leads to the variations in shape and size of the particles. Moreover, the phytochemistry of plant extracts changes with the seasonal and climatic variations, making it a concern for the precise reproducibility of the physical and chemical properties of the synthesized nanoparticle [9].

In the recent past, there is tremendous rise in the number of antimicrobial-resistant (AMR) pathogens in environment, food, and clinical settings. The problem has become so serious in healthcare that the number of global deaths caused by the infectious diseases are next to cardiovascular ailments and cancer [10]. Drug-resistant pathogens not only create new infections, but also worsen the treatment of chronic diseases in which the therapeutic effectiveness of antibiotics is reduced [11,12]. Moreover, if no proper action is taken, as per the speculations, the mortality caused by infectious diseases is expected to become the major reason for global deaths [13,14]. Hence, the onset of multiple-drug resistance is not only challenging for the human health, but also for the environment and livestock.

Biofilms are the microbial cells living inside the self-reduced matrix, mainly composed of natural plovers such as carbohydrates, proteins, DNA, etc. Biofilms are considered as hotspots and reservoirs for the antibiotic resistance genes [15]. The significance of biofilms can be predicted from the National Institute of Health (NIH) estimations which state that approximately 80% of infections are mainly supported by biofilms [16,17]. Most of the studies conducted before 2000 in antimicrobial drug discovery only considered the planktonic mode of microbial growth; however, the vast majority of bacteria in the environment and at infection sites live in biofilm mode. This has led researchers working in antibacterial drug discovery to revisit their approach and also consider the biofilms as potential drug target.

Certainly, there is a considerable gap in the development of newer antibiotics and the emergence of AMR. Owing to the risk of AMR development, researchers are focusing on reducing the virulence and pathogenicity, rather than trying to fully eliminate the microbes at inhibitory concentrations, as it creates selection pressure. Among such new antimicrobials, nanomaterials are widely being explored for such properties. In this article, ZnO-NPs were prepared using the extract of *Plumbago zeylanica*. The synthesized nanomaterials were characterized and their efficacy against the biofilms and related traits were assessed both on Gram –ve and Gram +ve bacteria.

2. Materials and Methods

2.1. Chemicals and Reagents

Acridine orange, zinc acetate, (MB116), glutaraldehyde solution, and microbiological media were obtained from HiMedia Laboratories, India. Crystal violet (CV) was purchased from SRL Pvt. Ltd., Mumbai, Maharashtra, India. Polystyrene plates were procured from Axiva Sichem Biotech, India.

2.2. Preparation of Plant Extract

The root powder of *Plumbago zeylanica* L. was obtained from Himalaya Drug Company, Dehradun, India. To make the root extract of *P. zeylanica*, 100 g powder was added to 1 L water (double-distilled) and then heated (50 °C) for 15 min. The suspension was kept for 3 h with intermittent shaking for proper extraction. The mixture was centrifuged, followed by filtration to obtain clear extract. Finally, extract was stored at −20 °C for further use.

2.3. Synthesis of ZnO-NPs

For green synthesis of zinc oxide nanoparticles (ZnO-NPs), an aqueous solution of zinc acetate was used as precursor. Briefly, 100 mL of plant extract was added drop by drop to 250 mL of 50 mM zinc acetate solution with continuous stirring using magnetic stirrer. The temperature of reaction mixture was fixed at 55 °C and the reaction was allowed to proceed for 3 h. Upon completion of reaction, ZnO-NPs were obtained by centrifugation at 15,000 rpm for 25 min. Lastly, the nanoparticles were dried in the oven at 80 °C and the powders were stored at room temperature for further use.

2.4. Characterization of ZnO-NPs

The initial characterization of ZnO-NPs was performed by recording its absorbance. The suspension of ZnO-NPs was made in water (double-distilled) by 30 min sonication. The UV–Vis absorbance of ZnO-NPs was recorded using spectrophotometer (Shimadzu, UV-1800, Kyoto City, Japan). The blank was set using water (double-distilled), and the absorption was recorded from 300 nm to 630 nm.

The crystal nature of ZnO-NPs was analyzed using X-ray diffraction (XRD). The diffraction pattern of the X-ray was taken using Cu-Kα radiation, and nickel monochromator was used as a source of light. ZnO-NPs size was calculated using the Debye–Scherrer equation. All prominent peaks were used for the calculation of the particle size of ZnO-NPs.

The chemical characterization of ZnO-NPs was carried out using Fourier-transform infrared spectroscopy (FTIR) to explore the vibrational and rotational property of the nanoparticle. The FTIR was recorded using spectrometer (Spectrum Two, Perkin Elmer Life, Waltham, MA, USA), at 1 cm^{-1} resolution in transmittance mode. The FTIR spectrum was taken from 4000 to 400 cm^{-1} [18].

Transmission electron microscopy was performed to analyze the size and shape of the green synthesized ZnO-NPs. TEM analysis was performed on a JOEL-2100 transmission electron microscope (Japan). The TEM grid was prepared by placing the aqueous suspension of ZnO-NPs on the TEM grid. The grid was air-dried overnight at room temperature before imaging. TEM images were taken at 200 kV and 50,000X magnification [19]. The particle size distribution analysis was carried out by calculating all nanoparticles in a frame and plotting their abundance against the size range. The morphology of ZnO-NPs was further analyzed by SEM analysis.

2.5. Bacteria Used and Their Culture Conditions

In this study, *Escherichia coli* ATCC 25922, *Pseudomonas aeruginosa* PAO1, and *Staphylococcus aureus* MTCC 3160 were used. The bacterial cultures were maintained and grown in Luria-Bertani (LB) broth unless stated. The biofilm-related experiments were performed at 37 °C.

2.6. Assays for the Inhibition of Biofilms

The inhibition of biofilms of the test bacteria was performed both quantitatively and on the solid surface. The detailed procedure of the biofilms in inhibition is described below.

2.6.1. Quantitative Inhibition of Biofilms by ZnO-NPs

The quantitative assessment of the biofilms development by ZnO-NPs was studied with crystal violet dye in 96-well polystyrene plates [20]. Two-fold dilutions of varying sub-MICs of ZnO-NPs were made in the wells of polystyrene plate in sterile LB broth. The bacteria were cultivated until log phase and diluted in Luria-Bertani broth for inoculum preparation. In the control group, no treatment with ZnO-NPs was given. The microtiter plate was incubated for 24 h in static incubator at 37 °C. Following incubation, wells of polystyrene plate were emptied and then gently washed three times with phosphate buffer (sterile) to remove the planktonic and loosely bound bacterial cells. Wells were then stained with crystal violet solution (0.1%) for 20 min. Excess amount of crystal violet was washed gently with sterile phosphate buffer followed by air-drying at room temperature for 20 min.

The crystal violet-stained wells solubilized in ethanol (90%) and OD of wells were recorded using microplate reader at 620 nm. The % inhibition was computed by comparing with respective control groups.

2.6.2. Inhibition of Biofilms on Solid Surface

The effect of ZnO-NPs on the biofilm-forming ability of test bacteria on glass surface was studied using microscopic tools such as confocal microscopy, light microscopy, and scanning electron microscopy. The detailed procedure for each microscopic analysis is described below.

Light Microscopic Analysis of Inhibition of Biofilms

The analysis of biofilm inhibition on glass surface was performed in a 24-well tissue culture plate [21]. The test bacteria were grown with respective highest sub-MIC of ZnO-NPs. The highest sub-MIC for *E. coli*, *S. aureus*, and *P. aeruginosa* were 100, 100, and 200 µg/mL, respectively. Briefly, ZnO-NPs were diluted to desired concentrations in LB broth in wells of a 24-well plate. Diluted log phase culture of bacteria was added as inoculum. Glass coverslips of 1 cm^2 were placed in slant position in each well, and plates were incubated at 24 h in a static incubator at 37 °C. The coverslips were removed and washed gently with buffer (phosphate) to remove the loosed attached cells. The biofilms were stained with crystal violet (0.1% aqueous solution) for 20 min followed by washing with the phosphate buffer. Finally, the glass coverslips were dried in air at room temperature and used for visualization. The visual inspection of biofilms was performed under light microscope equipped with a digital camera. The light microscopic images were taken at 40X.

Confocal Microscopic Analysis of Biofilms Inhibition

For confocal microscopic examination of biofilms, the bacteria were grown without and with ZnO-NPs as mentioned above in the light microscopic section. The biofilms of glass coverslips were given a gentle wash to eliminate the loosely attached bacteria cells and then stained with acridine orange (0.1%) for 30 min in the dark. The glass coverslips were washed to remove excess amount of the dye and then air-dried in the dark. The confocal microscopic analysis was performed using Zeiss LSM780 confocal laser scanning microscope, and the images were recorded at 63X.

Scanning Electron Microscopic Analysis of Biofilms Inhibition

For scanning electron microscopic (SEM) analysis of the biofilms inhibition, test bacteria were cultured, as mentioned above. After completion of incubation, glass coverslips were washed using autoclaved phosphate buffer. The biofilm of glass surface was fixed with 2.5% glutaraldehyde at 4 °C overnight. The biofilms were then dehydrated using ethanol gradient from 10% to 100% with each gradient for 15 min. Glass coverslips were dried followed by coating with gold. SEM images were taken using JOEL-JSM 6510 LV at 2000–2500X magnification and 15 kV.

2.7. Quantification of Exopolysaccharides (EPS) Inhibition by ZnO-NPs

The quantitative analysis of EPS inhibition was performed in cell-free supernatant of test bacterial cultures by estimating the sugar concentration [22]. In short, the bacteria were grown in the presence of varying respective sub-MICs of ZnO-NPs for 24 h at 37 °C. ZnO-NPs were diluted to the desired concentrations in culture tubes in Luria-Bertani broth. The diluted cultures form log phase was taken as inoculum. No treatment with ZnO-NPs was given in control group. After incubation, the cultures were centrifuged to obtain the cell-free supernatant. For the precipitation of EPS, 5 mL supernatant was mixed with 15 mL chilled ethanol and placed at 4 °C overnight. The levels of EPS in each treatment group and control group were estimated using standard Dubois method [23]. The percent inhibition was calculated by comparing with the respective control groups.

2.8. Eradication of the Established Biofilms by ZnO-NPs

The effect of ZnO-NPs was also tested on the established biofilms of the bacteria. In this assay, the biofilms were developed in 96-well polystyrene plates by incubating the cultures for 24 h without any treatment. The wells were then given a smooth wash with buffer (phosphate) to eliminate the loosely adhered and planktonic bacterial cells. Wells were again filled with fresh autoclaved LB broth, and ZnO-NPs were added to make desired concentrations. The multi-well plate was incubated for another 24 h in static condition. Wells of polystyrene plate were washed, and biofilms were stained, as mentioned in earlier. The OD of the wells were taken in 620 nm using a microplate reader. The data is presented as the percentage of biofilms left in treatment groups with respect to the control groups.

2.9. Statistical Analysis

All experiments were carried out in three independent replicates. The data is shown as average of replicates with the standard deviation. For statistical analysis, one-way ANOVA was carried out using Tukey test at 0.05 significance level. The post hoc analysis was performed to compare the means. The letters in different groups show varied significance groups which are in ascending/descending order starting from the letter "a".

3. Results and Discussion

3.1. Green Synthesis of ZnO-NPs and Its Characterization

The aqueous extract of *P. zeylanica* was used for the synthesis of zinc oxide nanoparticles. Zinc acetate solution was used as precursor for the synthesis. The addition of plant extract to zinc acetate solution resulted in precipitate formation. The ZnO-NPs synthesized using *P. zeylanica* extract were obtained by centrifugation followed by drying in hot air oven.

The initial characterization of ZnO-NPs was performed using UV–Vis spectroscopy. The absorption spectrum is presented in Figure 1A. ZnO-NPs exhibited a sharp absorption at 373 nm which is due to the surface plasmon resonance (SPR) and it is assigned to the intrinsic band-gap absorption of ZnO owing to the electron transitions from valance band to conduction band [24]. Our finding agrees with an earlier report in which ZnO-NPs synthesized using flower extract of *N. arbor-tristis* exhibited a sharp band at 365 nm [25]. Moreover, a study optimized the synthesis of ZnO-NPs, where the particles were prepared in three different conditions. The synthesized nanoparticles dried in vacuum at 30 °C did not exhibit any absorption peak from 300 to 600 nm. However, samples prepared by heating the zinc oxide nanoparticles at 60 °C and 100 °C showed the absorption maxima at 377 nm [26]. UV–Vis data suggested the formation of phases of ZnO NPs. The band-gap energy (E) of ZnO-NPs was computed using Planck's equation:

$$E = \frac{hc}{\lambda} \quad (1)$$

where h is Planck's constant, c is light velocity, and λ is light wavelength. The E (band-gap energy) for ZnO-NPs was found to be 3.326 eV, which is coherent with previous reports [27].

The crystal nature of ZnO-NPs was confirmed by analyzing X-ray diffraction. The ZRD pattern of ZnO-NPs is shown in Figure 1B. ZnO-NPs exhibited seven diffraction intense peaks at 31.09, 33.71, 35.56, 46.88, 55.96, 62.19, and 67.34 degrees. The detail of each peak is listed in Table 1. The most prominent peak was recorded at 35.56°. The narrow and sharp peaks denote that ZnO-NPs were well crystalline in nature. These peaks match with the JCPDS file number 361451 [26]. It is reported that ZnO-NPs synthesized using *N. arbor-tristis* extract exhibited XRD peaks at 31.80, 34.44, 36.24, 47.48, 56.62, 62.88, 66.42, and 68.0°, which were attributed to the hexagonal phase of zinc oxide [25]. Using the Debye–Scherrer equation (Equation (2)), the crystalline size of ZnO-NOPs was calculated [28]:

$$D = \frac{K\lambda}{\beta * cos\theta} \quad (2)$$

where D is size of the ZnO-NPs; β is full width of XRD peak at the half maximum; λ is wavelength (1.5406 Å) of radiation, and K is the Debye–Scherrer constant. The average size of ZNO-NPs was found to be 24.62 ± 2.74 nm. Moreover, the particle size calculated using the most intense peak (35.56°) was found to be 24.38 nm. The finding corroborates previous results in which the size of ZNO-NPs synthesized using *A. indica* extract was found to be 18 nm [24].

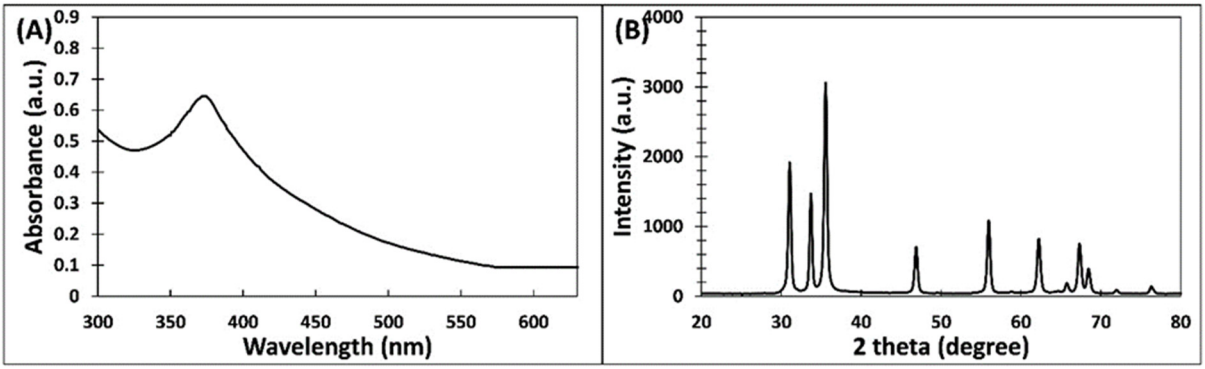

Figure 1. (**A**) UV–visible absorption spectrum of ZnO-NPs synthesized using *P. zeylanica* extract. (**B**) X-ray diffraction pattern of ZnO-NPs.

Table 1. Details of the most intense peaks of ZnO-NPs synthesized using *P. zeylanica* extract obtained from X-ray diffraction.

S. No.	2θ (degree)	Height (a.u.)	Area	FWHM	Size (nm)
1	31.090	2283.5	35,996.0	0.3219	25.61
2	33.719	1854.0	24,809.3	0.2789	29.76
3	35.566	3608.0	60,054.7	0.3421	24.38
4	46.880	833.0	14,037.3	0.3468	24.96
5	55.963	1288.7	23,612.0	0.3690	24.37
6	62.197	931.4	19,461.3	0.4272	21.71
7	67.340	852.0	18,560.0	0.4420	21.59
Average					24.62 ± 2.74

FWHM: Full width at half maximum; a.u.: arbitrary unit.

Transmission electron microscopy was performed to decipher the size and shape of ZnO-NPs. A TEM image of ZnO-NPs at 50,000X magnification is shown in Figure 2A. Most of the ZnO-NPs were irregular in shape with variation in sizes. The size of nanoparticles ranged from 8 to 40 nm (Figure 2B). Moreover, the morphological analysis of ZnO-NPs was performed by SEM analysis, and the micrograph is shown in Supplementary Figure S1. The nanoparticles were observed as spherical to oval or spheroidal in shape, further validating the TEM results. SEM images can be seen as huge clusters of particles as they were taken from the powdered form of ZnO-NPs. Variation in shape and size of green synthesized nanoparticles have been documented previously [25]. Such variation in the shape of green synthesized nanoparticles is due to the fact that some of the nanoparticles are capped and stabilized at lower size while other particles are stabilized at higher size. The phytocompounds present in extract of *P. zeylanica* are responsible for reduction of zinc and stabilization or capping of the particles. A similar report has been documented previously, where the size of ZnO-NPs ranged from 10 to 90 nm [29].

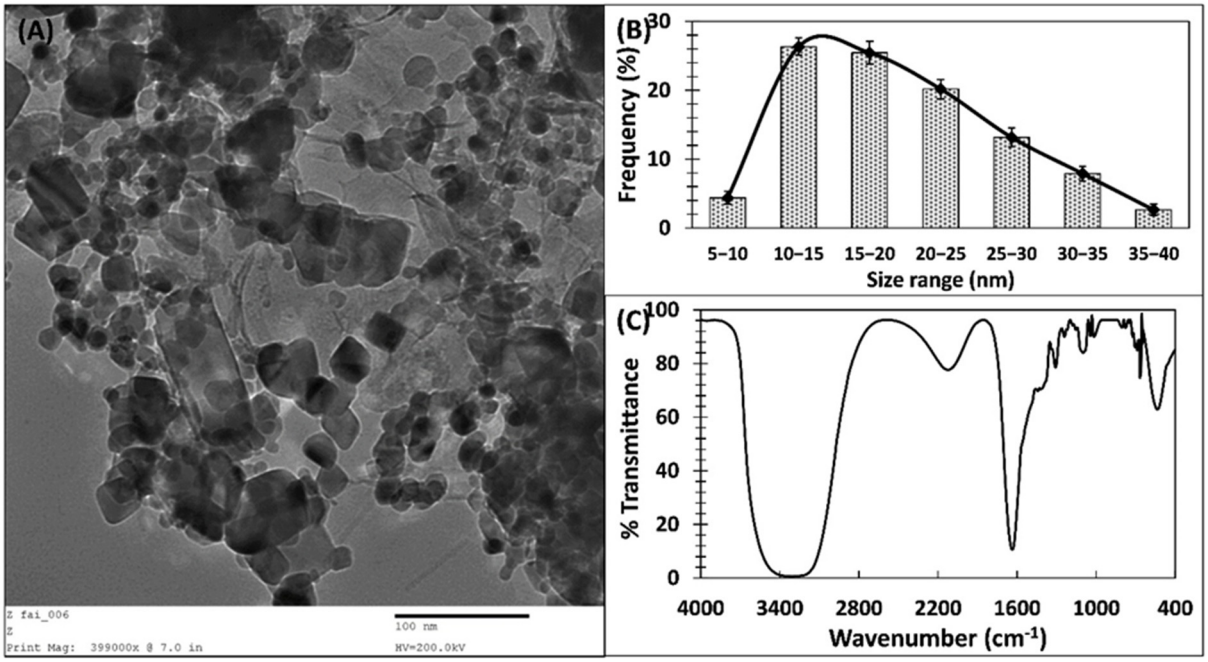

Figure 2. (**A**) Transmission electron micrograph of ZnO−NPs. (**B**) Particle size distribution histogram of ZnO−NPs. (**C**) Fourier-transform infrared spectrum of ZnO−NPs.

The chemical characterization of ZnO-NPs was performed using FTIR spectroscopy. The FTIR spectrum of ZnO-NPs is shown in Figure 2C. A sharp absorption band at 550 to 520 cm^{-1} confirms the presence of ZnO. The band ranging from 600 to 400 cm^{-1} is attributed to the M–O stretching (Zn–O) [30]. The absorption of zinc oxide nanoparticles at 457 cm^{-1} is reported in literature [24]. A very sharp and prominent peak at 1640 cm^{-1} is due to the amide I, showing that protein or enzyme of the *P. zeylanica* extract also contributes in the stabilization and capping of ZnO-NPs [31]. A broad peak at 3300 cm^{-1} is due the O–H stretching. The band at 2130 to 2110 cm^{-1} is related to stretching vibrations of C≡C of the alkynes [25]. The peaks near 1310 cm^{-1} are due to the aromatic amines. The glycosidic linkage of C–O–C was also reflected by peaks at 1230 cm^{-1} [32]. Overall, FTIR spectroscopy provided enough evidence regarding the role of phytoconstituents of *P. zeylanica* in the capping and stabilization of ZnO-NPs.

3.2. Inhibition of the Biofilm Development

ZnO-NPs were tested for biofilm inhibition against *E. coli*, *S. aureus,* and *P. aeruginosa*. First, the MIC of ZnO-NPs was obtained with broth dilution assay. The MIC of ZnO-NPs against *E. coli*, *P. aeruginosa*, and *S. aureus* was recorded to be 200, 400, and 200 µg/mL, respectively. The quantitative analysis of biofilms inhibition was performed and then qualitative examination of biofilms on glass surface was tested. The findings are discussed below.

3.2.1. Quantitative Analysis of Biofilms Inhibition

The effect of ZnO-NPs on the biofilms development of test bacteria was quantitatively studied using crystal violet assay in a 96-well polystyrene plate. The dose-dependent inhibition of biofilms formation is presented in Figure 3. Treatment with 1/16 × MIC, 1/8 × MIC, and 1/4 × MIC of ZnO-NPs reduced the biofilms development of *E. coli* by 15.80%, 27.48%, and 48.21%, respectively. In presence of highest sub-MIC (1/2 × MIC of Zn-NPs), there was more than 60% inhibition of *E. coli* biofilms. Likewise, the biofilm formation of *P. aeruginosa* was reduced by 30.86%, 48.83%, 54.59%, and 77.69% by the treatment of 1/16 × MIC, 1/8 × MIC, 1/4 × MIC, and 1/4 × MIC of ZnO-NPs, respectively. We also tested the effect of ZnO-NPs on the biofilms of a Gram + ve bacteria. At lower concentration

(1/16 × MIC), there was an insignificant inhibition of the biofilms of *S. aureus*. However, at higher sub-MICs (1/8 × MIC, 1/4 × MIC, and 1/2 × MIC of ZnO-NPs), the biofilms were significantly reduced where percent inhibition reached more than 70%. The results clearly show the biofilm inhibition potential of ZnO-NPs against the test bacteria.

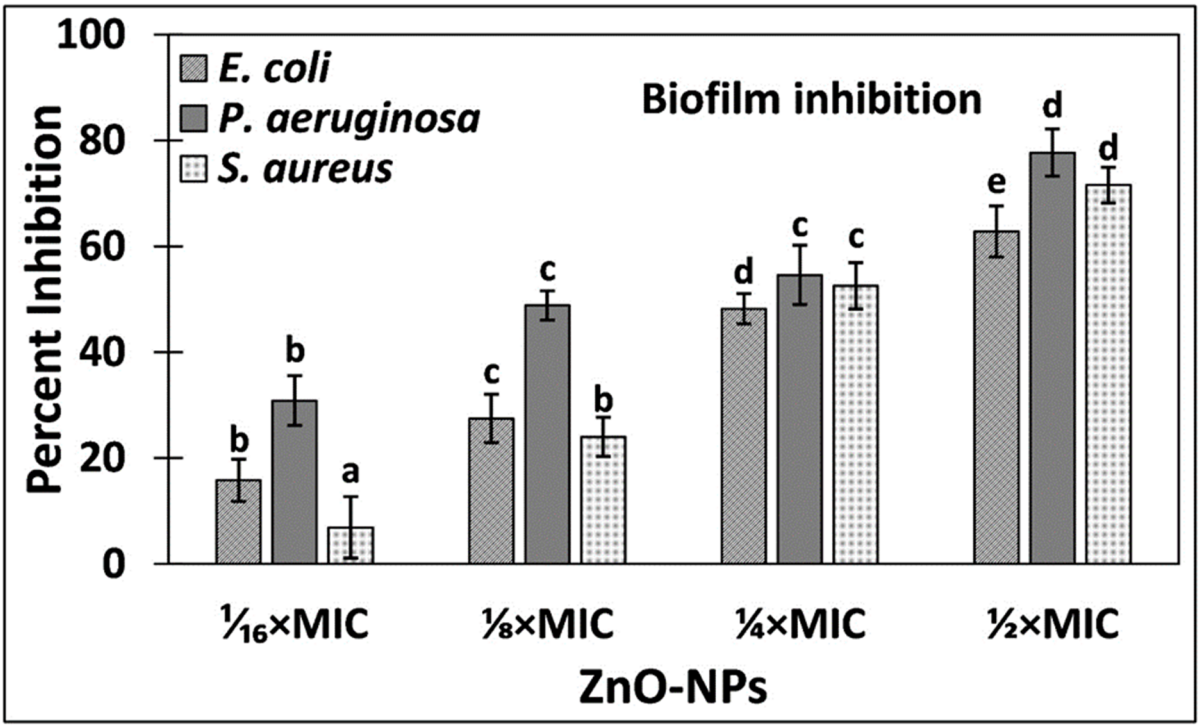

Figure 3. Inhibition of biofilm formation of *E. coli*, *P. aeruginosa*, and *S. aureus* by ZnO-NPs. Data is presented as average of three replicates and error bar is standard deviation. One-way ANOVA was performed using Tukey test at significance level of 0.05. Different letters in treatment groups represent different significance groups at *p*-value = 0.05 and are in ascending/descending order of values starting from the letter "a".

The incidence and worldwide spread of antimicrobial resistance both in clinical settings and the environment has posed serious concerns. The biofilms are considered as reservoirs of drug-resistant genes. Moreover, the horizontal gene transfer in biofilms leads to the rapid spread of antibiotic resistance [33]. In biofilms, there is limited entry of antibiotics and hence bacteria residing in biofilms are more tolerant and resistant to chemotherapeutic agents [15]. Considering the importance of biofilms in antibiotics resistance and clinical settings, targeting the bacteria biofilms is considered as a novel strategy in modern antimicrobial drug discovery. Our findings have shown that ZnO-NPs successfully inhibited the biofilm development of both Gram-negative and Gram-positive bacteria at sub-MICs. Previously, we have reported that zinc oxide nanoparticle synthesized using leaf extract of *Ochradenus baccatus* inhibited the biofilms development of *C. violaceum*, *P. aeruginosa*, *E. coli*, *K. pneumoniae*, *S. marcescens*, etc. at the sub-inhibitory concentrations [28]. Similarly, another study has reported that zinc oxide nanoparticles produce reactive oxygen species within cells of *P. aeruginosa* that also inhibit the biofilms development [34]. The nanoparticles are capable of interacting and diffusing on biofilms through the water channels that serve as transport passage for nutrients [35]. Additionally, the nanoparticles are adsorbed onto bacterial membrane and penetrate it, resulting in intracellular accumulation and killing of bacterial cells [36]. This explains the possible mechanism of antibiofilm activity of green synthesized ZnO-NPs.

3.2.2. Biofilm Inhibition by ZnO-NPs on the Glass Surface

The inhibition of biofilm development by ZnO-NPs of test bacteria was further explored on glass surface. The detailed analysis of the changes in biofilm architecture was studied using confocal microscopy, electron microscopy, and light microscopy. The findings are discussed below.

The preliminary qualitative examination of the biofilms inhibition on glass surface was performed using light microscopy. The light microscopic images of biofilms of test bacteria without and with highest respective sub-MICs of ZnO-NPs are shown in Figure 4. The micrographs show that there was dense biofilm formation on glass surface in the control groups of all bacteria. The bacteria were heavily colonized and can be seen as huge clumps of cells (Figure 4A,C,E). However, the treatment with 1/2 × MIC of ZnO-NPs remarkably reduced the biofilms formation on surface glass coverslips. Treatment with ZnO-NPs resulted in less colonization of cells to the solid support, and the bacteria were observed as scattered cells.

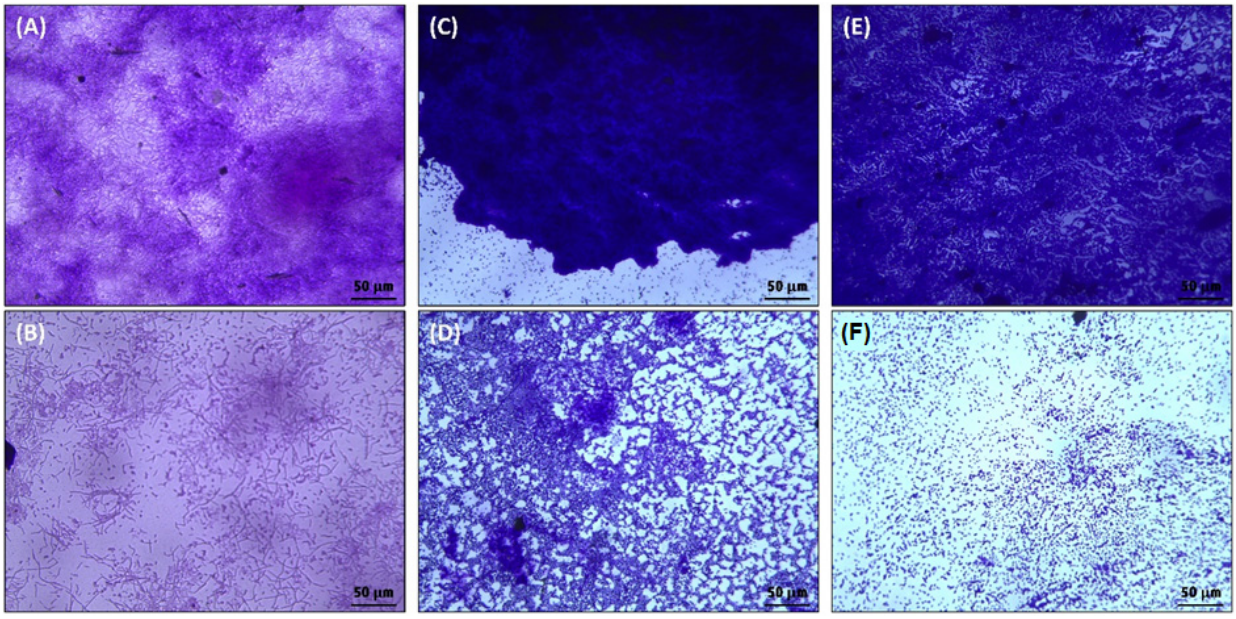

Figure 4. Light microscopic images of the *E. coli*, *P. aeruginosa*, and *S. aureus* biofilms in the absence and presence of ZnO-NPs. (**A**) untreated control *E. coli*; (**B**) *E. coli* treated with 1/2 × MIC of ZnO-NPs; (**C**) untreated control *P. aeruginosa*; (**D**) *P. aeruginosa* treated with 1/2 × MIC of ZnO-NPs; (**E**) untreated control *S. aureus*; (**F**) *S. aureus* treated with 1/2 × MIC of ZnO-NPs.

The confocal microscopic images of biofilms in the absence and presence of ZnO-NPs are shown in Figure 5. In control slides, all tested bacteria were found to be greatly colonized on the surface of glass coverslips. The bacteria were observed as thick mat-like structures of biofilms in many layers. On the contrary, ZnO-NPs reduced the bacterial biofilm development of solid support in which their colonization was extensively diminished. The bacteria in the treated group were found to be in scattered form and mostly as a single layer of cells on the surface of glass coverslips. These results agree with previous findings, where zinc oxide–xanthan gum nanocomposites reduced the biofilms formation of *C. violaceum* and *S. marcescens* as observed under confocal microscope [37].

The detailed examination of the changes in biofilm architecture by ZnO-NPs treatment was studied using scanning electron microscopy (SEM). SEM provides more detailed picture at higher magnification and enhanced resolution. The electron micrographs of the biofilms without and with ZnO-NPs is shown in Figure 6. Untreated *E. coli* was found to form strong biofilms on the surface of glass coverslips in which the bacterial morphology was observed to be smooth and normal. Moreover, some bacterial cells were also observed to be enclosed within the exopolymeric substances. However, the treatment with 1/2 × MIC of ZnO-NPs

resulted in reduced adherence of *E. coli* as evident from the limited colonization of bacterial cells. The presence of exopolymeric substances was also not observed. Similarly, in control slides of *P. aeruginosa* and *S. aureus*, the bacteria were found to be colonized and forming biofilms on the solid support. The presence of 1/2 × MIC of ZnO-NPs reduced the biofilms of both the bacteria in which a limited or reduced bacterial colonization was found. Based on the microscopic results, it became clear that ZnO-NPs not only inhibited the biofilms formation but also distorted the biofilm's architecture.

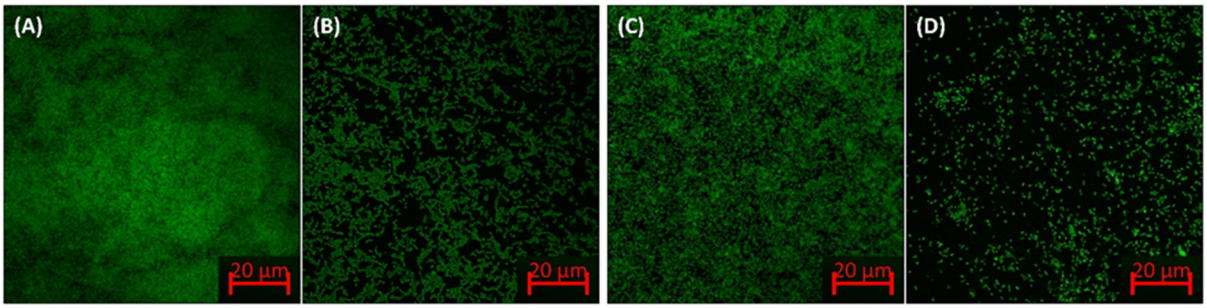

Figure 5. Confocal microscopic images of the *E. coli* and *P. aeruginosa* biofilms in the absence and presence of ZnO-NPs. (**A**) Untreated control *E. coli*; (**B**) *E. coli* treated with 1/2 × MIC of ZnO-NPs; (**C**) untreated control *P. aeruginosa*; (**D**) *P. aeruginosa* treated with 1/2 × MIC of ZnO-NPs.

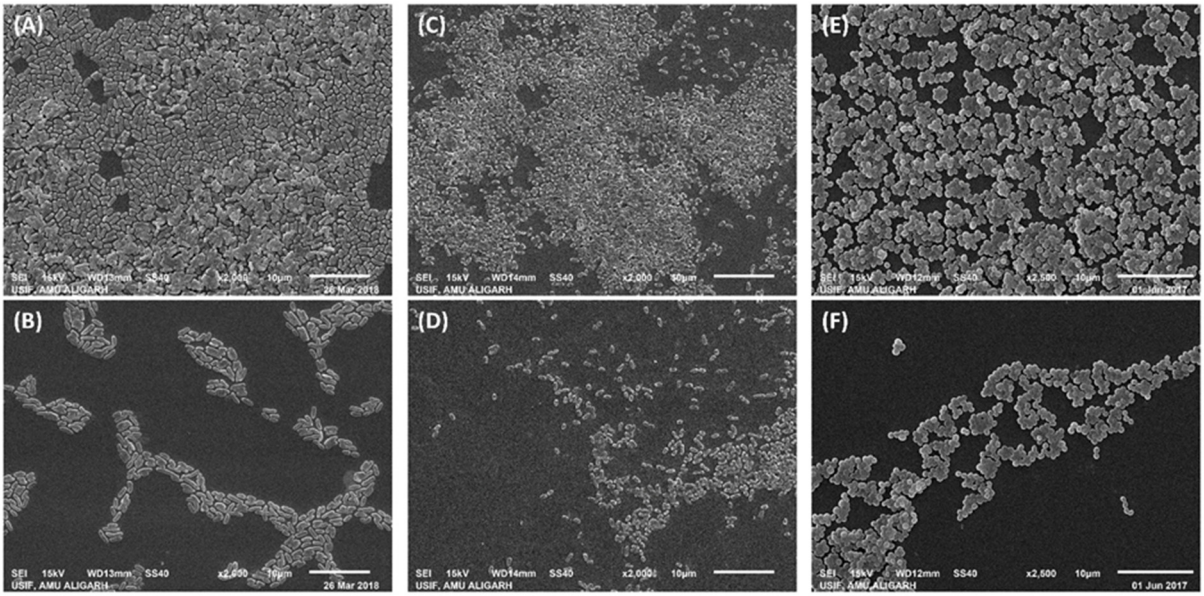

Figure 6. Scanning electron microscopic images of the *E. coli*, *P. aeruginosa*, and *S. aureus* biofilms in the absence and presence of ZnO-NPs. (**A**) Untreated control *E. coli*; (**B**) *E. coli* treated with 1/2 × MIC of ZnO-NPs; (**C**) untreated control *P. aeruginosa*; (**D**) *P. aeruginosa* treated with 1/2 × MIC of ZnO-NPs; (**E**) untreated control *S. aureus*; (**F**) *S. aureus* treated with 1/2 × MIC of ZnO-NPs.

The significance of the biofilms in clinical settings can be assessed from the National Institute of Health (NIH) and Centers for Disease Control and Prevention (CDC) United States data which estimates that the majority of microbial infections, including chronic infections, are associated with, and encouraged by, the biofilms [38]. Moreover, biofilms reduce the therapeutic efficacy of antibiotics and are also known as reservoirs of drug-resistant genes when horizontal gene transfer takes place [33]. This makes the biofilms an obvious target for the management of bacterial infections. A study has found that ZnO-NPs synthesized using leaf extract of *Ochradenus baccatus* inhibited the biofilms development of *C. violaceum*, *P. aeruginosa*, *E. coli*, *K. pneumoniae*, *S. marcescens*, etc. at the sub-MICs [28]. Zinc oxide–silver nanocomposites have also been reported to selectively target and reduce

the biofilms of *S. aureus*, *E. coli*, and *C. albicans* [39]. Moreover, green synthesized ZnO-NPs using seaweed were found to highly inhibit the biofilms of *B. licheniformis*, *E. coli*, *B. pumilus*, and *P. vulgaris* [40]. The findings indicate the possible application of ZnO-NPs to target the biofilms of bacterial pathogens, especially for surface coating and topical applications.

3.3. Inhibition of Exopolysaccharides (EPS) by ZnO-NPs

Exopolysaccharides (EPS) are one of the major components of exopolymeric substances that constitute biofilms [41]. Moreover, such polymeric substances are polymers of natural origin that provide structural integrity and framework to the biofilms [42]. Being a fundamental component, extracellular polymeric substance also plays a crucial role in the determination of physicochemical properties of the biofilms. EPS serves as barrier for the entry of chemotherapeutic agents, including antibiotics, by blocking their entry in the biofilms [41]. The levels of EPS in the absence and presence of ZnO-NPs are shown in Figure 7A. The EPS secretion in *S. aureus* was reduced by 14.44%, 26.58%, 42.86%, and 61.24% by the treatment of 1/16 × MIC, 1/8 × MIC, 1/4 × MIC, and 1/2 × MIC of ZnO-NPs, respectively. Similarly, the presence of 1/16 × MIC, 1/8 × MIC, 1/4 × MIC, and 1/2 × MIC of ZnO-NPs inhibited the EPS production of *P. aeruginosa* by 19.83%, 33.77%, 55.40%, and 67.96%, respectively. The EPS of *E. coli* was maximally inhibited in which more than 73% inhibition was recorded. The secretion of EPS not only provides integrity to the biofilm architecture but also confers resistance against the antibiotics [43]. Due to the positive correlation between the EPS secretion biofilm formation, the inhibition of EPS is also considered as an alternative target to mitigate the biofilms of pathogenic bacteria [44]. Our results corroborate with earlier findings in which zinc oxide nanoparticles synthesized using leaf extract of *O. baccatus* inhibited the EPS production of *P. aeruginosa*, *K. pneumonia*, *E. coli*, *L. monocytogenes*, *S. marcescens*, and *C. violaceum* at sub-MICs [28]. The inhibition of EPS production may result in exposure of bacterial biofilms cells that may assist in the eradication of biofilms. Our findings confirm that green synthesized ZnO-NPs successfully reduced the EPS production both in Gram-positive and Gram-negative bacteria.

3.4. Eradication of Established Biofilms of Pathogenic Bacteria by ZnO-NPs

Although most of the nanoparticles have been proven to be effective against the planktonic bacterial growth, among them, few are known to inhibit the biofilms of bacterial pathogens. However, a limited spectrum of antibiotics has been found that are successful in eradicating the established biofilms. Here, the effect of ZnO-NPs on the preformed biofilms of the bacteria was also tested, and the results are presented in Figure 7B. In the presence of 1/16 × MIC, 1/8 × MIC, 1/4 × MIC, and 1/2 × MIC of ZnO-NPs, the established biofilm of *E. coli* was reduced by 10.26%, 19.71%, 41.05%, and 52.69%, respectively. Similarly, the preformed biofilms of *S. aureus* were decreased by 19.31%, 28.46%, 48.29%, and 59.79% by the treatment of 1/16 × MIC, 1/8 × MIC, 1/4 × MIC, and 1/2 × MIC of ZnO-NPs, respectively. The maximum eradication was recorded in *P. aeruginosa,* in which more than 65% eradication of the established biofilms was found. The major constituents of the biofilms are polypeptides, polysaccharides, nucleic acids, etc., that not only provide framework to the biofilms but also restrict the entry of antibiotics into biofilms [45]. ZnO-NPs were also found to inhibit the EPS production of the test bacteria. The reduction in EPS secretion exposed the bacterial cells residing in biofilms that could have ultimately resulted in eradication of the biofilms. Pancreatin-doped zinc oxide nanoparticles have been found to eradicate the established biofilms of *S. aureus* (methicillin resistant) [46]. Moreover, silver nanoparticles prepared using *Withania somnifera* have also been documented to mitigate the performed biofilms of *S. aureus*, *S. mutans*, *P. aeruginosa*, and *S. typhimurium* [47]. Silver nanoparticles have been found to diffuse and penetrate the matrix of bacterial biofilms [35]. The diffusion of ZnO-NPs inside the matrix of the biofilms may also be one of the possible mechanisms of the eradication of biofilms. Based on the findings of this study, it is obvious that ZnO-NPs were potent both in inhibiting and eradicating the biofilms of pathogenic bacteria.

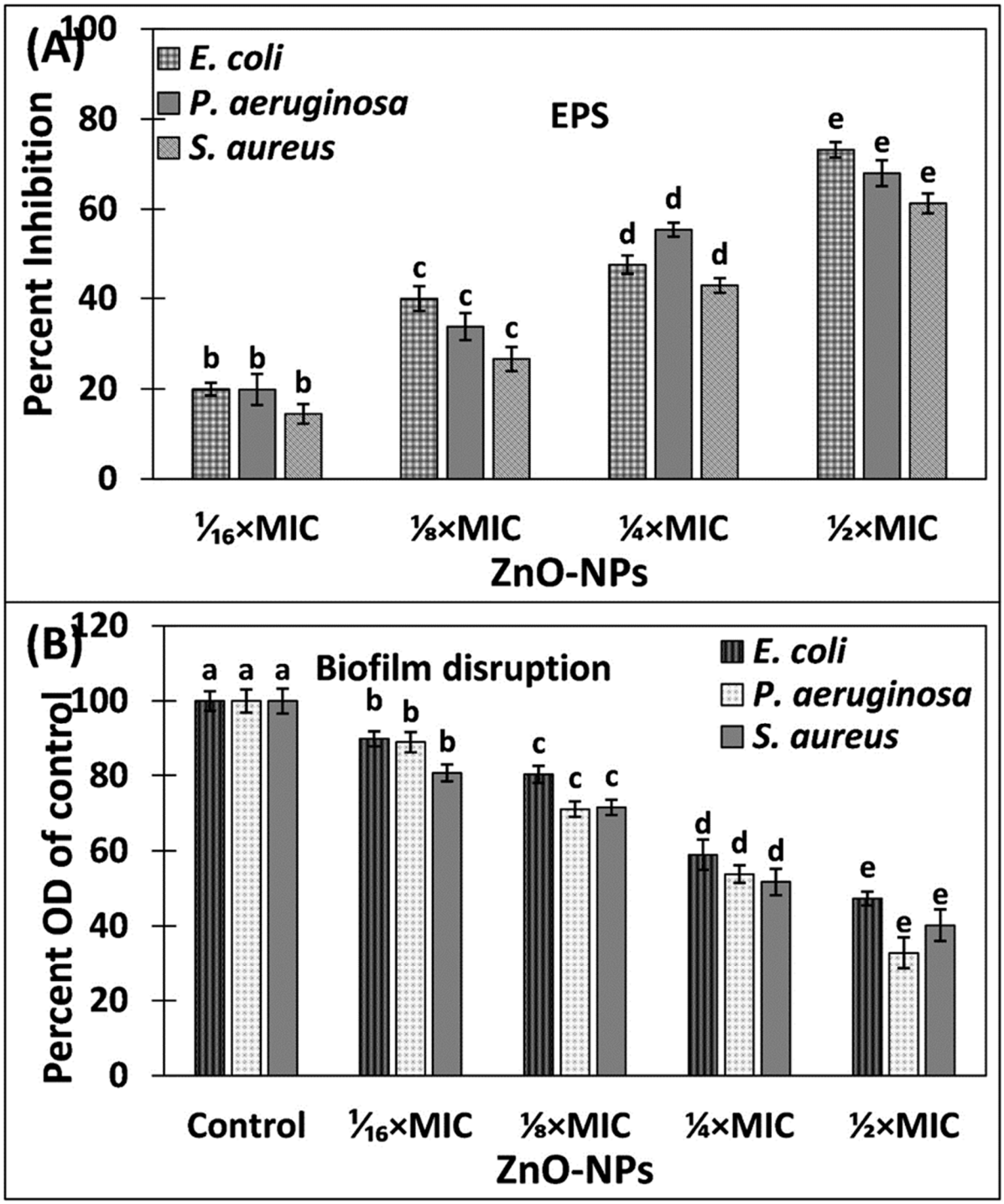

Figure 7. (**A**) Inhibition of EPS production in *E. coli*, *P. aeruginosa*, and *S. aureus* by ZnO-NPs. (**B**) Eradication of established biofilms of *E. coli*, *P. aeruginosa*, and *S. aureus* by ZnO-NPs. Data is presented as average of three replicates, and error bar is standard deviation. One-way ANOVA was performed using Tukey test at significance level of 0.05. Different letters in treatment groups represent different significance groups at p-value = 0.05 and are in ascending/descending order of values starting from the letter "a".

4. Conclusions

The global incidence and emergence of drug-resistant microbes has created a need for the development of novel strategies to tackle microbial infections. Among new approaches, the screening or development of biofilm inhibitors is considered a novel target. In this

study, ZnO-NPs were synthesized using the aqueous extract of *P. zeylanica* and then characterized. ZnO-NPs inhibited the biofilms development and EPS production of *P. aeruginosa*, *S. aureus*, and *E. coli* in a dose-dependent manner. Moreover, ZnO-NPs altered the biofilm's architecture and reduced the attachment and colonization bacteria onto the solid surface. The eradication of biofilms was also achieved in the presence of ZnO-NPs. The results of this study show the potency of ZnO-NPs against the biofilm-forming ability of bacterial pathogens that may be used as a biofilm inhibitor after careful in vivo investigation, at least for topical applications and coating of medical devices.

Supplementary Materials: The following supporting information can be downloaded at: https://www.mdpi.com/article/10.3390/app12020710/s1, Figure S1: SEM images of ZnO-NPs synthesized using aqueous extract of *Plumbago zeylanica*.

Author Contributions: Conceptualization, I.A. and F.M.H.; methodology, F.M.H., F.A.Q., M.J.H., M.H.B., J.M.K., and N.A.A.-S. software, F.A.Q., and F.M.H.; formal analysis, F.M.H., F.A.Q., M.J.H., M.H.B., J.M.K., and N.A.A.-S.; investigation, F.M.H., F.A.Q., M.J.H., M.H.B., J.M.K., and N.A.A.-S.; data curation, F.M.H., F.A.Q., M.J.H., M.H.B., J.M.K., and N.A.A.-S.; writing—original draft preparation, F.M.H., F.A.Q. and I.A.; writing—review and editing, F.M.H., F.A.Q. and I.A.; supervision, I.A. and F.M.H. All authors have read and agreed to the published version of the manuscript.

Funding: The research received no funding.

Institutional Review Board Statement: Not Applicable.

Informed Consent Statement: Not applicable.

Data Availability Statement: The data presented in this study are available on request from the corresponding author.

Acknowledgments: Authors are grateful to the Researchers Supporting Project Number (RSP-2021/360), King Saud University, Riyadh, Saudi Arabia.

Conflicts of Interest: The authors declare that there are no conflict of interest associated with this study.

Abbreviations

AMR	Antimicrobial resistant
EPS	Exopolysaccharides
FTIR	Fourier-transform infrared spectroscopy
MIC	Minimum Inhibitory concentration
SEM	Scanning electron microscopy
TEM	Transmission electron microscopy
XRD	X-ray diffraction
ZnO-NPs	Zinc oxide nanoparticles

References

1. Khare, S.; Williams, K.; Gokulan, K. Nanotechnology. In *Encyclopedia of Food Microbiology*; Elsevier: Amsterdam, The Netherlands, 2014; pp. 893–900.
2. Qamar, S.A.; Asgher, M.; Khalid, N.; Sadaf, M. Nanobiotechnology in health sciences: Current applications and future perspectives. *Biocatal. Agric. Biotechnol.* **2019**, *22*, 101388. [CrossRef]
3. Khan, I.; Saeed, K.; Khan, I. Nanoparticles: Properties, applications and toxicities. *Arab. J. Chem.* **2019**, *12*, 908–931. [CrossRef]
4. Iravani, S. Green synthesis of metal nanoparticles using plants. *Green Chem.* **2011**, *13*, 2638. [CrossRef]
5. Baig, N.; Kammakakam, I.; Falath, W. Nanomaterials: A review of synthesis methods, properties, recent progress, and challenges. *Mater. Adv.* **2021**, *2*, 1821–1871. [CrossRef]
6. Joerger, R.; Klaus, T.; Granqvist, C.G. Biologically Produced Silver-Carbon Composite Materials for Optically Functional Thin-Film Coatings. *Adv. Mater.* **2000**, *12*, 407–409. [CrossRef]
7. Chauhan, R.P.; Charu, G.; Dhan, P. Methodological advancements in green nanotechnology and their applications in biological synthesis of herbal nanoparticles. *Int. J. Bioassays* **2012**, *1*, 6–10.
8. Ingale, A.G. Biogenic Synthesis of Nanoparticles and Potential Applications: An Eco- Friendly Approach. *J. Nanomed. Nanotechnol.* **2013**, *4*, 165. [CrossRef]

9. Mukherjee, S.; Patra, C.R. Biologically synthesized metal nanoparticles: Recent advancement and future perspectives in cancer theranostics. *Futur. Sci. OA* **2017**, *3*, FSO203. [CrossRef]
10. WHO The Top 10 Causes of Death; 2018. Available online: https://www.who.int/news-room/fact-sheets/detail/the-top-10-causes-of-death (accessed on 27 November 2021).
11. Shakoor, S.; Platts-Mills, J.A.; Hasan, R. Antibiotic-Resistant Enteric Infections. *Infect. Dis. Clin. N. Am.* **2019**, *33*, 1105–1123. [CrossRef]
12. Andleeb, S.; Majid, M.; Sardar, S. Environmental and public health effects of antibiotics and AMR/ARGs. In *Antibiotics and Antimicrobial Resistance Genes in the Environment*; Elsevier: Amsterdam, The Netherlands, 2020; pp. 269–291.
13. Dadgostar, P. Antimicrobial Resistance: Implications and Costs. *Infect. Drug Resist.* **2019**, *12*, 3903–3910. [CrossRef]
14. WHO No Time to Wait: Securing the Future from Drug-Resistant Infections; 2019. Available online: https://www.who.int/docs/default-source/documents/no-time-to-wait-securing-the-future-from-drug-resistant-infections-en.pdfsfvrsn=5b424d7_6 (accessed on 27 November 2021).
15. Balcázar, J.L.; Subirats, J.; Borrego, C.M. The role of biofilms as environmental reservoirs of antibiotic resistance. *Front. Microbiol.* **2015**, *6*, 1216. [CrossRef]
16. Donlan, R.M. Biofilm Formation: A Clinically Relevant Microbiological Process. *Clin. Infect. Dis.* **2001**, *33*, 1387–1392. [CrossRef] [PubMed]
17. Schachter, B. Slimy business—The biotechnology of biofilms. *Nat. Biotechnol.* **2003**, *21*, 361–365. [CrossRef] [PubMed]
18. Al-Shabib, N.A.; Husain, F.M.; Ahmad, N.; Qais, F.A.; Khan, A.; Khan, A.; Khan, M.S.; Khan, J.M.; Shahzad, S.A.; Ahmad, I. Facile Synthesis of Tin Oxide Hollow Nanoflowers Interfering with Quorum Sensing-Regulated Functions and Bacterial Biofilms. *J. Nanomater.* **2018**, *2018*, 6845026. [CrossRef]
19. Ahmed, A.S.; Iqbal, A.; Shafi, A.; Qais, F.A.; Ahamad, T.; Srivastava, S. Enhanced Removal of Crystal Violet Dye and Anti-Biofilm Activity of Ti Doped CeO_2 Nanoparticles Synthesized by Phoenix Dactylifera Mediated Green Method. *J. Clust. Sci.* **2020**, *32*, 1723–1737. [CrossRef]
20. O'Toole, G.A.; Kolter, R. Flagellar and twitching motility are necessary for Pseudomonas aeruginosa biofilm development. *Mol. Microbiol.* **1998**, *30*, 295–304. [CrossRef]
21. Qais, F.A.; Ahmad, I.; Altaf, M.; Manoharadas, S.; Al-Rayes, B.F.; Ali Abuhasil, M.S.; Almaroai, Y.A. Biofabricated silver nanoparticles exhibit broad-spectrum antibiofilm and antiquorum sensing activity against Gram-negative bacteria. *RSC Adv.* **2021**, *11*, 13700–13710. [CrossRef]
22. Qais, F.A.; Khan, M.S.; Ahmad, I. Broad-spectrum quorum sensing and biofilm inhibition by green tea against gram-negative pathogenic bacteria: Deciphering the role of phytocompounds through molecular modelling. *Microb. Pathog.* **2019**, *126*, 379–392. [CrossRef]
23. DuBois, M.; Gilles, K.A.; Hamilton, J.K.; Rebers, P.A.; Smith, F. Colorimetric Method for Determination of Sugars and Related Substances. *Anal. Chem.* **1956**, *28*, 350–356. [CrossRef]
24. Elumalai, K.; Velmurugan, S. Green synthesis, characterization and antimicrobial activities of zinc oxide nanoparticles from the leaf extract of *Azadirachta indica* (L.). *Appl. Surf. Sci.* **2015**, *345*, 329–336. [CrossRef]
25. Jamdagni, P.; Khatri, P.; Rana, J.S. Green synthesis of zinc oxide nanoparticles using flower extract of Nyctanthes arbor-tristis and their antifungal activity. *J. King Saud. Univ. Sci.* **2018**, *30*, 168–175. [CrossRef]
26. Bala, N.; Saha, S.; Chakraborty, M.; Maiti, M.; Das, S.; Basu, R.; Nandy, P. Green synthesis of zinc oxide nanoparticles using Hibiscus subdariffa leaf extract: Effect of temperature on synthesis, anti-bacterial activity and anti-diabetic activity. *RSC Adv.* **2015**, *5*, 4993–5003. [CrossRef]
27. Rajiv, P.; Rajeshwari, S.; Venckatesh, R. Bio-Fabrication of zinc oxide nanoparticles using leaf extract of Parthenium hysterophorus L. and its size-dependent antifungal activity against plant fungal pathogens. *Spectrochim. Acta Part A Mol. Biomol. Spectrosc.* **2013**, *112*, 384–387. [CrossRef]
28. Al-Shabib, N.A.; Husain, F.M.; Hassan, I.; Khan, M.S.; Ahmed, F.; Qais, F.A.; Oves, M.; Rahman, M.; Khan, R.A.; Khan, A.; et al. Biofabrication of Zinc Oxide Nanoparticle from Ochradenus baccatus Leaves: Broad-Spectrum Antibiofilm Activity, Protein Binding Studies, and In Vivo Toxicity and Stress Studies. *J. Nanomater.* **2018**, *2018*, 8612158. [CrossRef]
29. Khatami, M.; Alijani, H.Q.; Heli, H.; Sharifi, I. Rectangular shaped zinc oxide nanoparticles: Green synthesis by Stevia and its biomedical efficiency. *Ceram. Int.* **2018**, *44*, 15596–15602. [CrossRef]
30. Sangeetha, G.; Rajeshwari, S.; Venckatesh, R. Green synthesis of zinc oxide nanoparticles by aloe barbadensis miller leaf extract: Structure and optical properties. *Mater. Res. Bull.* **2011**, *46*, 2560–2566. [CrossRef]
31. Shankar, S.S.; Ahmad, A.; Sastry, M. Geranium Leaf Assisted Biosynthesis of Silver Nanoparticles. *Biotechnol. Prog.* **2003**, *19*, 1627–1631. [CrossRef]
32. Khan, Z.R.; Khan, M.S.; Zulfequar, M.; Shahid Khan, M. Optical and Structural Properties of ZnO Thin Films Fabricated by Sol-Gel Method. *Mater. Sci. Appl.* **2011**, *2*, 340–345. [CrossRef]
33. Abe, K.; Nomura, N.; Suzuki, S. Biofilms: Hot spots of horizontal gene transfer (HGT) in aquatic environments, with a focus on a new HGT mechanism. *FEMS Microbiol. Ecol.* **2020**, *96*, fiaa031. [CrossRef]
34. Dwivedi, S.; Wahab, R.; Khan, F.; Mishra, Y.K.; Musarrat, J.; Al-Khedhairy, A.A. Reactive oxygen species mediated bacterial biofilm inhibition via zinc oxide nanoparticles and their statistical determination. *PLoS ONE* **2014**, *9*, e111289. [CrossRef]

35. Peulen, T.O.; Wilkinson, K.J. Diffusion of nanoparticles in a biofilm. *Environ. Sci. Technol.* **2011**, *45*, 3367–3373. [CrossRef] [PubMed]
36. Ansari, M.A.; Khan, H.M.; Khan, A.A.; Cameotra, S.S.; Saquib, Q.; Musarrat, J. Gum arabic capped-silver nanoparticles inhibit biofilm formation by multi-drug resistant strains of Pseudomonas aeruginosa. *J. Basic Microbiol.* **2014**, *54*, 688–699. [CrossRef] [PubMed]
37. Husain, F.M.; Hasan, I.; Qais, F.A.; Khan, R.A.; Alam, P.; Alsalme, A. Fabrication of Zinc Oxide-Xanthan Gum Nanocomposite via Green Route: Attenuation of Quorum Sensing Regulated Virulence Functions and Mitigation of Biofilm in Gram-Negative Bacterial Pathogens. *Coatings* **2020**, *10*, 1190. [CrossRef]
38. Jamal, M.; Ahmad, W.; Andleeb, S.; Jalil, F.; Imran, M.; Nawaz, M.A.; Hussain, T.; Ali, M.; Rafiq, M.; Kamil, M.A. Bacterial biofilm and associated infections. *J. Chinese Med. Assoc.* **2018**, *81*, 7–11. [CrossRef]
39. Rosenberg, M.; Visnapuu, M.; Vija, H.; Kisand, V.; Kasemets, K.; Kahru, A.; Ivask, A. Selective antibiofilm properties and biocompatibility of nano-ZnO and nano-ZnO/Ag coated surfaces. *Sci. Rep.* **2020**, *10*, 13478. [CrossRef]
40. Ishwarya, R.; Vaseeharan, B.; Kalyani, S.; Banumathi, B.; Govindarajan, M.; Alharbi, N.S.; Kadaikunnan, S.; Al-anbr, M.N.; Khaled, J.M.; Benelli, G. Facile green synthesis of zinc oxide nanoparticles using Ulva lactuca seaweed extract and evaluation of their photocatalytic, antibiofilm and insecticidal activity. *J. Photochem. Photobiol. B Biol.* **2018**, *178*, 249–258. [CrossRef]
41. Sauer, K.; Camper, A.K. Characterization of Phenotypic Changes inPseudomonas putida in Response to Surface-Associated Growth. *J. Bacteriol.* **2001**, *183*, 6579–6589. [CrossRef]
42. Maunders, E.; Welch, M. Matrix exopolysaccharides; the sticky side of biofilm formation. *FEMS Microbiol. Lett.* **2017**, *364*. [CrossRef]
43. Yildiz, F.H.; Schoolnik, G.K. Vibrio cholerae O1 El Tor: Identification of a gene cluster required for the rugose colony type, exopolysaccharide production, chlorine resistance, and biofilm formation. *Proc. Natl. Acad. Sci. USA* **1999**, *96*, 4028–4033. [CrossRef]
44. Czaczyk, K.; Myszka, K. Biosynthesis of Extracellular Polymeric Substances (EPS) and Its Role in Microbial Biofilm Formation. *Polish J. Environ. Stud.* **2007**, *16*, 799–806.
45. Høiby, N.; Ciofu, O.; Johansen, H.K.; Song, Z.; Moser, C.; Jensen, P.Ø.; Molin, S.; Givskov, M.; Tolker-Nielsen, T.; Bjarnsholt, T. The clinical impact of bacterial biofilms. *Int. J. Oral Sci.* **2011**, *3*, 55–65. [CrossRef] [PubMed]
46. Banerjee, S.; Vishakha, K.; Das, S.; Dutta, M.; Mukherjee, D.; Mondal, J.; Mondal, S.; Ganguli, A. Antibacterial, anti-biofilm activity and mechanism of action of pancreatin doped zinc oxide nanoparticles against methicillin resistant Staphylococcus aureus. *Colloids Surf. B Biointerfaces* **2020**, *190*, 110921. [CrossRef] [PubMed]
47. Qais, F.A.; Samreen; Ahmad, I. Broad-spectrum inhibitory effect of green synthesised silver nanoparticles from *Withania somnifera* (L.) on microbial growth, biofilm and respiration: A putative mechanistic approach. *IET Nanobiotechnology* **2018**, *12*, 325–335. [CrossRef]